Computers & Structures Vol. 28, No. 3, pp. 407–419, 1988
Printed in Great Britain.

0045-7949/88 $3.00 + 0.00

PLATE BENDING ANALYSIS USING MACRO ELEMENTS

J. PETROLITO and B. W. GOLLEY
Department of Civil Engineering, University College, Australian Defence Force Academy, Campbell, ACT, Australia

(*Received* 21 *March* 1987)

Abstract—A variable degree of freedom plate bending element is presented. The displacement function within an element satisfies the governing thin plate equation, substantially reducing the number of equations requiring generation and solution for the accurate analysis of beam–slab structures. Large elements corresponding to structural units bounded by beams may be used, requiring a minimum of data preparation. The examples considered show that engineering accuracy may be obtained with the generation and solution of very few equations. In addition, a modified version of the ACM element with conforming displacements is shown to be a sub-element of the proposed element.

INTRODUCTION

The development of finite elements for the analysis of plate bending problems has remained an active area of research since the first plate bending element was introduced some 27 years ago. In a recent review [1], Hrabok and Hrudley catalogued 88 different plate bending elements. These elements were derived using a variety of approaches and a number of different theories for both thin and thick plates.

Despite the available finite elements, it is however uncommon to analyse beam–slab–column structures using finite elements [2], and most structures are analysed using approximate methods. For example, building frames in which the floor slabs act integrally with beams are usually analysed as frames, with the floor slab contributing some approximately determined stiffness to the beams.

Accurate analysis of beam–slab–column structures requires the use of finite element methods, with the structure discretised into a large number of elements, in which in-plane and out-of-plane displacements are considered. For structures of general geometry, triangular or isoparametric elements are used. However, many structures, including bridges and multi-storey buildings, are laid out in a rectangular pattern and rectangular elements are an obvious choice for use with these structures. A range of rectangular plate bending elements is available of which the twelve degree of freedom non-conforming ACM element [3] and the sixteen degree of freedom conforming element [4] are the best known. Rectangular elements for in-plane forces are among the simplest elements, with a number being discussed by Zienkiewicz [3]. In this paper, only plate bending is considered, while the effects of in-plane forces will be the subject of a future paper.

To reduce the number of elements required for solving plate bending problems, several panel elements have been proposed. Gutkowski and Wang [5] proposed a 'finite panel' in which displacements are combinations of trigonometric and hyperbolic functions. The method, however, was restricted to symmetrical loadings and plates continuous over rigid supports. Golley [6] and Yan [7, 8] have proposed variable degree of freedom panel elements in which transverse displacements and normal moments are continuous between elements. The elements produce accurate results with minimum discretisation, but the mixed degrees of freedom, consisting of transverse displacement and normal moment coefficients, are difficult to incorporate into beam–slab structures.

The term macro element has been used to describe a finite element suitable for modelling a domain with minimum discretisation [9]. In the present paper, a variable degree of freedom rectangular plate bending macro element and an associated beam element are described. Isotropic plates are considered for brevity although extension to orthotropic plates is straightforward. In general, each plate element corresponds to a structural unit bounded by beams, permitting discretisation into a minimum number of elements. The plate elements are restricted to having constant thickness, which is not considered a severe limitation in practical cases.

Distinctive features of the present work include:

(1) The element displacement function satisfies the governing differential equation, greatly reducing the number of equations requiring solution for engineering accuracy.

(2) C_1 continuity at element corners is achieved by careful selection of shape functions. The degrees of freedom at plate corners enable conventional elements to be used for columns.

(3) The elements have variable degrees of freedom which enable convergence to be readily assessed. Degrees of freedom associated with the sides of an

element may be varied from side to side enabling elements with large aspect ratios to be treated economically.

(4) Unlike existing plate bending macro elements, the proposed element is formulated with displacement degrees of freedom. This enables the proposed element to be easily combined with other elements. In particular, the element can be combined with an analogous plane stress element, enabling beam–slab systems which include the effects of in-plane stresses to be analysed efficiently [10].

THIN PLATE THEORY

The plate is assumed to behave according to thin plate theory [11]. Under the assumptions of thin plate theory, the deformed shape of a plate is completely described by the deflection of the middle surface, w, which is a function of x and y only.

The state of strain in the plate is described by the curvature vector, $\boldsymbol{\kappa} = \{\kappa_{xx}\ \kappa_{yy}\ \kappa_{xy}\}$, given by

$$\boldsymbol{\kappa} = -\mathbf{D}^T(w), \tag{1}$$

where

$$\mathbf{D} = \lfloor \partial^2/\partial x^2 \quad \partial^2/\partial y^2 \quad 2\partial^2/\partial x \partial y \rfloor. \tag{2}$$

The moment distribution in the plate is described by the moment vector, $\mathbf{M} = \{M_x\ M_y\ M_{xy}\}$. For an isotropic plate, the moment–curvature relationship is

$$\mathbf{M} = \mathbf{E}\boldsymbol{\kappa}, \tag{3}$$

where

$$\mathbf{E} = D\begin{bmatrix} 1 & \nu & 0 \\ \nu & 1 & 0 \\ 0 & 0 & (1-\nu)/2 \end{bmatrix} \tag{4}$$

$$D = \frac{Eh^3}{12(1-\nu^2)}. \tag{5}$$

E is Young's modulus, ν is Poisson's ratio and h is the plate thickness.

By considering the forces on a differential element of the plate as shown in Fig. 1(a), the equilibrium

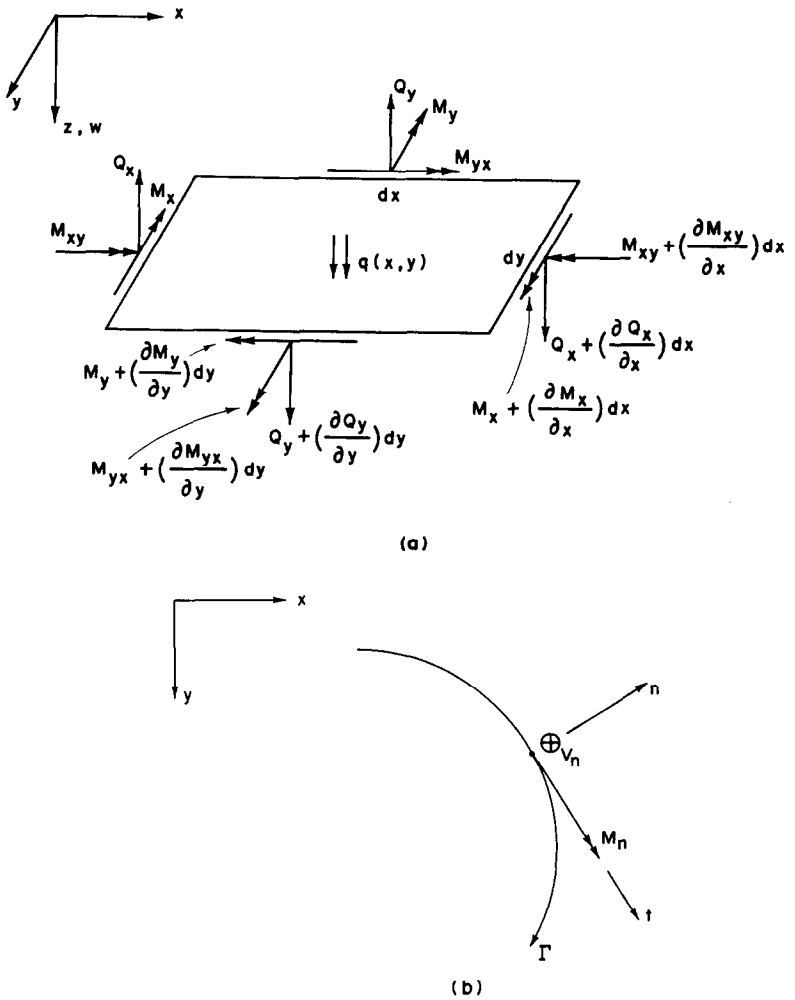

Fig. 1. Thin plate theory—notation. (a) Differential element of plate. (b) Portion of plate boundary.

equation for the plate is obtained as

$$\mathbf{DM} + q = 0. \tag{6}$$

Combining eqns (1), (3) and (6) gives the governing differential equation for the plate, namely

$$\nabla^4 w = w_{,xxxx} + 2w_{,xxyy} + w_{,yyyy} = \frac{q}{D}, \tag{7}$$

where a comma denotes partial differentiation.

Fig. 1(b) shows a portion of the boundary, Γ, of the plate. The boundary conditions specified on Γ are

$$\text{either } w = \bar{w} \quad \text{or} \quad V_n = \bar{V}_n \tag{8}$$

and

$$\text{either } w_{,n} = \bar{w}_{,n} \quad \text{or} \quad M_n = \bar{M}_n, \tag{9}$$

where the normal moment, M_n, and the effective shear, V_n, are given by

$$M_n = -D[w_{,xx} + w_{,yy} - (1-\nu)w_{,tt}] \tag{10}$$

and

$$V_n = -D[w_{,xxn} + w_{,yyn} + (1-\nu)w_{,ntt}]. \tag{11}$$

ELEMENT DISPLACEMENT FUNCTIONS

In a typical element, e, shown in Fig. 2, the displacement, w^e, is approximated by

$$w^e = \mathbf{N}_p^e(x,y)\boldsymbol{\phi}_p^e + \sum_{m=1}^{M} \mathbf{N}_{tm}^e(x,y)\boldsymbol{\phi}_{tm}^e + \sum_{m=1}^{M^*} \mathbf{N}_{nm}^e(x,y)\boldsymbol{\Phi}_{nm}^e + w_o^e(x,y) \tag{12}$$

or

$$w^e = w_p^e + w_t^e + w_n^e + w_o^e. \tag{13}$$

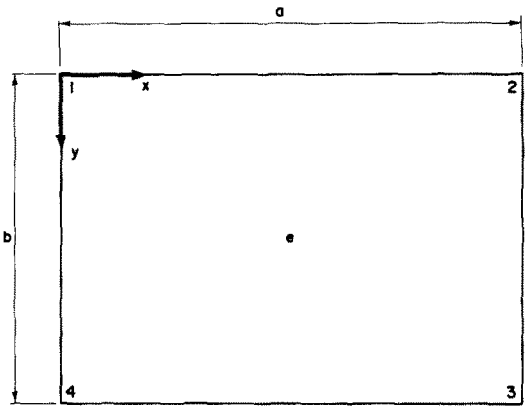

Fig. 2. Typical macro element.

The four terms in eqn (12) are obtained by superposing the cases shown in Fig. 3. In the figure, the symbol S denotes a simple support (i.e. $w = M_n = 0$).

The first term in eqn (12) involves polynomial functions only. The terms of $\mathbf{N}_p^e(x,y)$ are shape functions identical to those of the ACM element and

$$\boldsymbol{\phi}_p^e = \{w_1^e\ w_2^e\ w_3^e\ w_4^e\ \theta_{x1}^e\ \theta_{y1}^e\ \theta_{x2}^e\ \theta_{y2}^e\ \theta_{x3}^e\ \theta_{y3}^e\ \theta_{x4}^e\ \theta_{y4}^e\} \tag{14}$$

are the element degrees of freedom shown in Fig. 3(a). The terms in $\mathbf{N}_p^e(x,y)$ satisfy the homogenous form of eqn (7), and are given by Zienkiewicz [3]. The corner displacments, $w_1^e \ldots w_4^e$, are common to adjacent elements while the corner rotations, $\theta_{x1}^e \ldots \theta_{y4}^e$, are local to the element. During elimination of the rotation variables, which is discussed later, the first term is required in partitioned form, namely

$$w_p^e = \lfloor \mathbf{N}_{p1}^e\ \mathbf{N}_{p2}^e \rfloor \begin{Bmatrix} \boldsymbol{\phi}_{p1}^e \\ \boldsymbol{\phi}_{p2}^e \end{Bmatrix}, \tag{15}$$

where

$$\boldsymbol{\phi}_{p1}^e = \{w_1^e\ w_2^e\ w_3^e\ w_4^e\} \tag{16}$$

and

$$\boldsymbol{\phi}_{p2}^e = \{\theta_{x1}^e\ \theta_{y1}^e\ \theta_{x2}^e\ \theta_{y2}^e\ \theta_{x3}^e\ \theta_{y3}^e\ \theta_{x4}^e\ \theta_{y4}^e\}. \tag{17}$$

The second term in eqn (12) results from sine series boundary displacements with boundary normal moments zero, as shown in Fig. 3(b). On the sides of the element, the displacement is approximated by

$$\begin{aligned} w_t^e(x,0) &= \sum_{m=1}^{M} \phi_{tm12}^e \sin\left(\frac{m\pi x}{a}\right) \\ w_t^e(a,y) &= \sum_{m=1}^{M} \phi_{tm23}^e \sin\left(\frac{m\pi y}{b}\right) \\ w_t^e(x,b) &= \sum_{m=1}^{M} \phi_{tm34}^e \sin\left(\frac{m\pi x}{a}\right) \\ w_t^e(0,y) &= \sum_{m=1}^{M} \phi_{tm14}^e \sin\left(\frac{m\pi y}{b}\right). \end{aligned} \tag{18}$$

The coefficients $\phi_{tm12}^e \ldots \phi_{tm14}^e$ in eqn (18) are common to adjacent elements. The subscripts 12, 23, etc. refer to sides between corner nodes 1 and 2, 2 and 3 etc. The upper limits of the sine series in eqn (18) may, in general, vary on different sides of the element. This would lead to computational efficiency in some cases. However, for simplicity, it is assumed that the same number of terms is taken on each side of the element.

With boundary displacements specified by eqn (18) and with normal moments zero on the boundaries, Levy series solutions [11] of the homogeneous form of eqn (7) can be obtained in terms of the coefficients

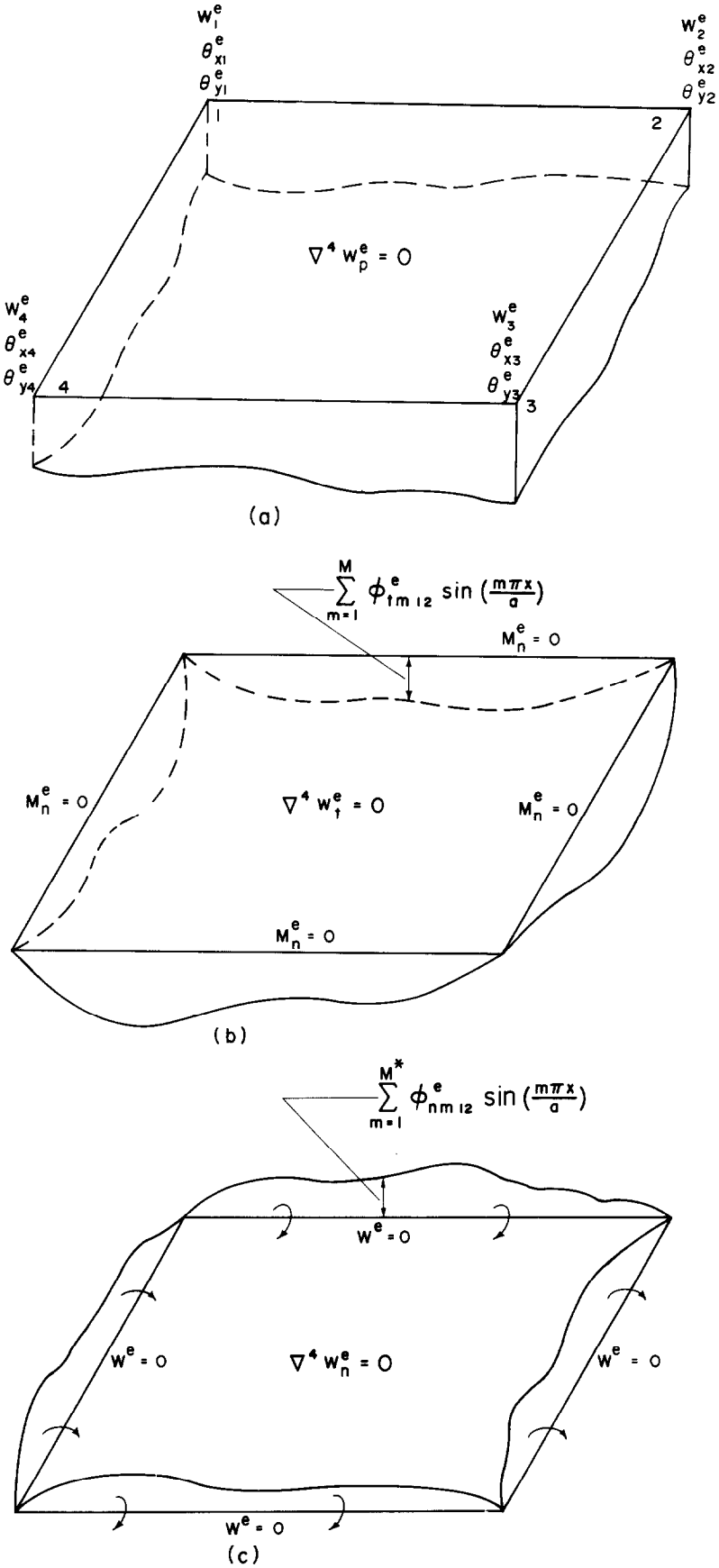
w_1^e
θ_{x1}^e
θ_{y1}^e
w_2^e
θ_{x2}^e
θ_{y2}^e
1
2
$\nabla^4 w_p^e = 0$
w_4^e
θ_{x4}^e
θ_{y4}^e
w_3^e
θ_{x3}^e
θ_{y3}^e
4
3
(a)
$\sum_{m=1}^{M} \phi_{tm12}^e \sin\left(\frac{m\pi x}{a}\right)$
$M_n^e = 0$
$M_n^e = 0$
$\nabla^4 w_t^e = 0$
$M_n^e = 0$
$M_n^e = 0$
(b)
$\sum_{m=1}^{M^*} \phi_{nm12}^e \sin\left(\frac{m\pi x}{a}\right)$
$w^e = 0$
$w^e = 0$
$\nabla^4 w_n^e = 0$
$w^e = 0$
$w^e = 0$
(c)

Fig. 3

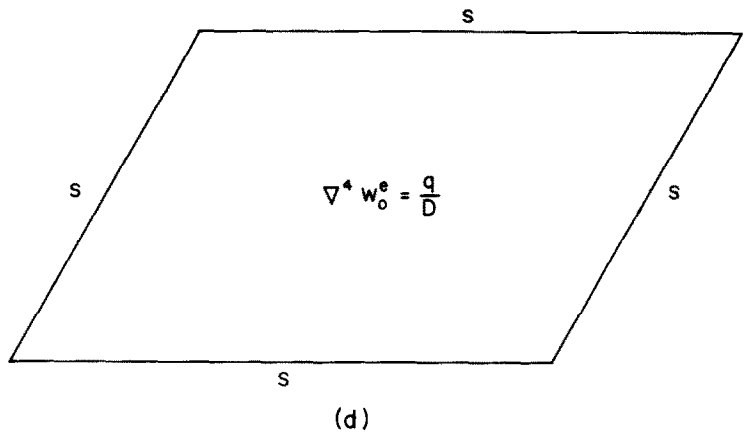

Fig. 3. Displacement approximation within element.

ϕ^e_{im12}, ϕ^e_{im23}, ϕ^e_{im34}, and ϕ^e_{im14}. Hence for the *mth* term in the series, the displacement is given by

$$w^e_{im} = \mathbf{N}^e_{im}(x, y)\boldsymbol{\phi}^e_{im}, \tag{19}$$

where

$$\boldsymbol{\phi}^e_{im} = \{\phi^e_{im12}\ \phi^e_{im23}\ \phi^e_{im34}\ \phi^e_{im14}\}. \tag{20}$$

The terms in $\mathbf{N}^e_{im}(x, y)$ are given in the Appendix. Summing the solutions in eqn (19) for all m gives the second term in eqn (12).

The third term in eqn (12) is the displacement due to the application of normal boundary moments in the form of sine series as shown in Fig. 3(c), with boundary displacements zero. On the sides of the element, the normal moments are approximated by

$$M^e_{yn}(x, 0) = \sum_{m=1}^{M^*} \phi^e_{nm12} \sin\left(\frac{m\pi x}{a}\right)$$

$$M^e_{xn}(a, y) = -\sum_{m=1}^{M^*} \phi^e_{nm23} \sin\left(\frac{m\pi y}{b}\right)$$

$$M^e_{yn}(x, b) = -\sum_{m=1}^{M^*} \phi^e_{nm34} \sin\left(\frac{m\pi x}{a}\right)$$

$$M^e_{xn}(0, y) = \sum_{m=1}^{M^*} \phi^e_{nm14} \sin\left(\frac{m\pi y}{b}\right). \tag{21}$$

The coefficients $\phi^e_{nm12} \ldots \phi^e_{nm14}$ are not common to adjacent elements. The number of terms in the sine series in eqn (21) is taken to be the same on all sides of the element but need not be equal to the number of terms in eqn (18). The signs in eqn (21) have been chosen to simplify the formulation of the element stiffness matrix as is shown below.

With boundary moments specified by eqn (21) and with displacements zero on the boundaries, Levy series solutions of the homogeneous form of eqn (7) can be obtained in terms of the coefficients ϕ^e_{nm12}, ϕ^e_{nm23}, ϕ^e_{nm34} and ϕ^e_{nm14}. Hence for the mth term in the series, the displacement is given by

$$w^e_{nm} = \mathbf{N}^e_{nm}(x, y)\boldsymbol{\phi}^e_{nm}, \tag{22}$$

where

$$\boldsymbol{\phi}^e_{nm} = \{\phi^e_{nm12}\ \phi^e_{nm23}\ \phi^e_{nm34}\ \phi^e_{nm14}\}. \tag{23}$$

The terms in $\mathbf{N}^e_{nm}(x, y)$ are given in the Appendix. Summing the solutions in eqn (22) for all m gives the third term in eqn (12).

The last term in eqn (12) is a particular solution of eqn (7) with all sides of the element simply supported as shown in Fig. 3(d). For the most general loading, Navier's double series solution is required, while Levy's single series solution may be used in more restricted loading cases [11]. The displacement w^e given by eqn (12) satisfies the governing differential equation [eqn (7)].

ESTABLISHMENT OF C_1 CONTINUITY

C_1 continuity is enforced in two stages. Firstly, C_1 continuity is exactly enforced at element corners by introducing rotation variables at the corners which are common to adjacent elements. Element variables $\boldsymbol{\phi}^e_{p2}$ are eliminated at the element level.

Secondly, C_1 continuity is approximately established on element sides by introducing new variables which are weighted integrals of side normal rotations. The moment coefficients, $\boldsymbol{\phi}^e_{nm}$, which are not common to adjacent elements, are then eliminated.

Establishment of C_1 *continuity at corners*

From eqns (12) and (15), the total rotations at the element corners, $\boldsymbol{\theta}^e$, are given by

$$\boldsymbol{\theta}^e = \boldsymbol{\phi}^e_{p2} + \sum_{m=1}^{M} \mathbf{A}^e_m \boldsymbol{\phi}^e_{im}, \tag{24}$$

where

$$\boldsymbol{\theta}^e = \{w^e_{,x1}\ w^e_{,y1}\ w^e_{,x2}\ w^e_{,y2}\ w^e_{,x3}\ w^e_{,y3}\ w^e_{,x4}\ w^e_{,y4}\} \tag{25}$$

and the terms in the transformation matrix $\mathbf{A}^e_m$ are given in the Appendix. Eliminating the variables $\boldsymbol{\phi}^e_{p2}$ using eqn (24) and substituting into eqn (12) gives the element displacement as

$$w^e = \lfloor \mathbf{N}^e_{p1}\ \mathbf{N}^e_{p2} \rfloor \begin{Bmatrix} \boldsymbol{\phi}^e_{p1} \\ \boldsymbol{\theta}^e \end{Bmatrix} + \sum_{m=1}^{M} \bar{\mathbf{N}}^e_{tm} \boldsymbol{\phi}^e_{tm} + \sum_{m=1}^{M^*} \mathbf{N}^e_{nm} \boldsymbol{\phi}^e_{nm} + w^e_o \quad (26)$$

or

$$w^e = \mathbf{N}^e_p \bar{\boldsymbol{\phi}}^e_p + \sum_{m=1}^{M} \bar{\mathbf{N}}^e_{tm} \boldsymbol{\phi}^e_{tm} + \sum_{m=1}^{M^*} \mathbf{N}^e_{nm} \boldsymbol{\phi}^e_{nm} + w^e_o, \quad (27)$$

where

$$\bar{\mathbf{N}}^e_{tm} = \mathbf{N}^e_{tm} - \mathbf{N}^e_{p2} \mathbf{A}^e_m. \quad (28)$$

Establishment of C_1 *continuity on sides*

One way to achieve the continuity of normal rotations, in an integral sense, is by using the modified principle of total potential energy originally derived by Jones [12]. In this approach, Lagrange multipliers are introduced along the interelement boundaries so that the continuity of normal rotations becomes a natural boundary condition. These Lagrange multipliers can be interpreted as interelement normal moments [13]. Harvey and Kelsey [14] first used this approach to derive a triangular plate bending element. The disadvantage of this approach is that the final variables are mixed, consisting of both displacement and force variables, making it difficult to incorporate beam elements.

An alternative variational principle which leads to a displacement formulation was derived by Tong [15]. In this approach, interelement normal rotations and element boundary normal moments are introduced which are independent of the element quantities. The new interelement normal rotations are continuous between elements while the new boundary normal moments are local to the elements and are eliminated at the element level. Tong's variational principle also leads to the continuity of normal rotations as a natural boundary condition.

In this work, a technique based on a weighted integral approach, which results in a displacement formulation, is used. The weighted integral approach highlights the manner in which the continuity of normal rotations is achieved. In this approach, new variables, which are weighted integrals of side normal rotations and are common to adjacent elements, are introduced. By eliminating the element moment variables, which are not common to adjacent elements, the total potential energy is obtained in terms of displacement and rotation variables only.

ELEMENT FORMULATION

From eqn (27), the element displacement can be written as

$$w^e = \mathbf{N}^e(x, y)\boldsymbol{\phi}^e + w^e_o(x, y), \quad (29)$$

where

$$\mathbf{N}^e = \lfloor \mathbf{N}^e_p\ \bar{\mathbf{N}}^e_{t1}\ \bar{\mathbf{N}}^e_{t2} \ldots \bar{\mathbf{N}}^e_{tM}\ \mathbf{N}^e_{n1}\ \mathbf{N}^e_{n2} \ldots \mathbf{N}^e_{nM^*} \rfloor \quad (30)$$

and

$$\boldsymbol{\phi}^e = \{\bar{\boldsymbol{\phi}}^e_p\ \boldsymbol{\phi}^e_{t1}\ \boldsymbol{\phi}^e_{t2} \ldots \boldsymbol{\phi}^e_{tM}\ \boldsymbol{\phi}^e_{n1}\ \boldsymbol{\phi}^e_{n2} \ldots \boldsymbol{\phi}^e_{nM^*}\}. \quad (31)$$

Using eqn (29), displacements and forces around the boundary of element e can be obtained as

$$\begin{aligned} w^e(t) &= \mathbf{N}^e_w(t)\boldsymbol{\phi}^e \\ w^e_{,n}(t) &= \mathbf{N}^e_\theta(t)\boldsymbol{\phi}^e + w^e_{,no}(t) \\ M^e_n(t) &= \mathbf{N}^e_M(t)\boldsymbol{\phi}^e \\ V^e_n(t) &= \mathbf{N}^e_V(t)\boldsymbol{\phi}^e + V^e_{no}(t), \end{aligned} \quad (32)$$

where the terms $w^e_{,no}(t)$ and $V^e_{no}(t)$ arise from the particular solution for the applied loading. Since the particular solution is associated with simple supports around the element boundary, there are no particular solution terms for w^e and M^e_n.

The total potential energy of the region under analysis is

$$\Pi_p = \sum_e \left(\frac{1}{2} \int_{A^e} \mathbf{M}^{eT} \boldsymbol{\kappa}^e \, \mathrm{d}A - \int_{A^e} q^e w^e \, \mathrm{d}A - \int_{\Gamma^e_p} (\bar{M}^e_n w^e_{,n} + \bar{V}^e_n w^e) \, \mathrm{d}\Gamma \right), \quad (33)$$

where A^e is the area of element e and Γ^e_p is the portion of the boundary of element e where force boundary conditions are specified. Note that the integral of $\bar{V}^e_n$ over Γ^e_p also includes the contribution of any corner forces [11]. As eqn (7) is satisfied within each element, the area integral in the first term of eqn (33) can be converted to a boundary integral by the use of Clapeyron's theorem [11], i.e.

$$\int_{A^e} \mathbf{M}^{eT} \boldsymbol{\kappa}^e \, \mathrm{d}A = \int_{A^e} q^e w^e \, \mathrm{d}A + \int_{\Gamma^e} (M^e_n w^e_{,n} + V^e_n w^e) \, \mathrm{d}\Gamma, \quad (34)$$

where Γ^e is the boundary of the element and the integral of V^e_n includes the contributions of any corner forces. Combining eqns (33) and (34) gives

$$\Pi_p = \sum_e \left(\frac{1}{2} \int_{\Gamma^e} (M^e_n w^e_{,n} + V^e_n w^e) \, \mathrm{d}\Gamma - \frac{1}{2} \int_{A^e} q^e w^e \, \mathrm{d}A - \int_{\Gamma^e_p} (\bar{M}^e_n w^e_{,n} + \bar{V}^e_n w^e) \, \mathrm{d}\Gamma \right). \quad (35)$$

Substituting eqns (29) and (32) into eqn (35) gives

$$\Pi_p = \sum_e \left(\frac{1}{2} \boldsymbol{\phi}^{eT} \mathbf{K}^e \boldsymbol{\phi}^e - \boldsymbol{\phi}^{eT} \mathbf{R}^e + \text{constant} \right), \quad (36)$$

where

$$\mathbf{K}^e = \int_{\Gamma^e} (\mathbf{N}_M^{eT}\mathbf{N}_\theta^e + \mathbf{N}_V^{eT}\mathbf{N}_w^e)\,d\Gamma$$

$$\mathbf{R}^e = \frac{1}{2}\int_{A^e} q^e \mathbf{N}^{eT} dA - \frac{1}{2}\int_{\Gamma^e} (w^e_{,no}\mathbf{N}_M^{eT} + V^e_{no}\mathbf{N}_w^{eT})\,d\Gamma + \int_{\Gamma_p^e} (\bar{M}_n \mathbf{N}_\theta^{eT} + \bar{V}_n \mathbf{N}_w^{eT})\,d\Gamma \quad (37)$$

and the constant arises from terms which only involve the particular solution and is independent of ϕ^e. $\mathbf{K}^e$ is a symmetrical matrix.

The expression for $\mathbf{R}^e$ in eqn (37) can be simplified by use of Betti's theorem [11], which leads to the equation

$$\int_{A^e} q^e \mathbf{N}^{eT} dA + \int_{\Gamma^e} V^e_{no}\mathbf{N}_w^{eT} d\Gamma = \int_{\Gamma^e} w^e_{,no}\mathbf{N}_M^{eT} d\Gamma. \quad (38)$$

Combining eqns (37) and (38) gives

$$\mathbf{R}^e = \int_{A^e} q^e \mathbf{N}^{eT} dA - \int_{\Gamma^e} w^e_{,no}\mathbf{N}_M^{eT} d\Gamma + \int_{\Gamma_p^e} (\bar{M}_n \mathbf{N}_\theta^{eT} + \bar{V}_n \mathbf{N}_w^{eT})\,d\Gamma. \quad (39)$$

The terms in $\mathbf{K}^e$ and $\mathbf{R}^e$ have been evaluated explicitly in order to avoid numerical integration [10]. $\mathbf{K}^e$ contains the stiffness matrix of the ACM element as a submatrix.

The twelve terms in $\mathbf{R}^e$ associated with $\bar{\phi}_p^e$ contain infinite series terms which arise from the particular solution, w_o^e. For the most general loading, double infinite series terms arise. However for more restricted types of loadings, only single infinite series terms arise. In the remaining terms of $\mathbf{R}^e$, infinite series terms are avoided by noting certain identities from Betti's theorem.

Neglecting the constant, eqn (36) can be written in partitioned form as

$$\Pi_p = \sum_e \left(\frac{1}{2}\{\phi_i^e\ \phi_j^e\}^T \begin{bmatrix} \mathbf{K}_{ii}^e & \mathbf{K}_{ij}^e \\ \mathbf{K}_{ij}^{eT} & \mathbf{K}_{jj}^e \end{bmatrix} \begin{Bmatrix} \phi_i^e \\ \phi_j^e \end{Bmatrix} - \{\phi_i^e\ \phi_j^e\}^T \begin{Bmatrix} \mathbf{R}_i^e \\ \mathbf{R}_j^e \end{Bmatrix}\right), \quad (40)$$

where

$$\phi_i^e = \{\bar{\phi}_p^e\ \phi_{i1}^e\ \phi_{i2}^e \ldots \phi_{iM}^e\} \quad (41)$$

and

$$\phi_j^e = \{\phi_{n1}^e\ \phi_{n2}^e \ldots \phi_{nM^*}^e\}. \quad (42)$$

To enforce continuity of normal rotations on the sides of the element, weighted integrals of normal rotation are introduced as follows. On the side $y = 0$ of element e, weighted integrals of normal rotation, ϕ^e_{n12m}, are defined as

$$\phi^e_{n12m} = \int_0^a \lambda^e\left(\frac{x}{a}\right)\left(w^e_{,y}(x,0) - w^e_{,y1}\left(1-\frac{x}{a}\right) - w^e_{,y2}\left(\frac{x}{a}\right)\right)dx, \quad (43)$$

where

$$\lambda\left(\frac{x}{a}\right) = \left\{\sin\left(\frac{\pi x}{a}\right)\sin\left(\frac{2\pi x}{a}\right)\ldots\sin\left(\frac{(M^*-2)\pi x}{a}\right) \times\left(1-\frac{x}{a}\right)\left(\frac{x}{a}\right)\right\}, \quad M^* \geq 2$$

$$\lambda\left(\frac{x}{a}\right) = \left\{\left(1-\frac{x}{a}\right)\left(\frac{x}{a}\right)\right\}, \quad M^* = 2 \quad (44)$$

$$\lambda\left(\frac{x}{a}\right) = \left\{\sin\left(\frac{\pi x}{a}\right)\right\}, \quad M^* = 1. \quad (44)$$

In eqn (43), a linear function of the two end rotations, $w^e_{,y1}$ and $w^e_{,y2}$, which are continuous between adjacent elements, has been subtracted from the total normal rotation on the side. This is not necessary for the development of the element and the weighted integrals could have been alternatively defined as

$$\phi^e_{n12m} = \int_0^a \lambda^e\left(\frac{x}{a}\right) w^e_{,y}(x,0)\,dx. \quad (45)$$

The use of either the definition in eqn (43) or (45) together with the procedure detailed below leads to identical results. However, the definition in eqn (43) is used in preference since it simplifies the formulation of the associated beam element and leads directly to a modified ACM element as discussed later.

Following the definition in eqn (43), weighted integrals of normal rotations on the other three sides of the element are defined as

$$\phi^e_{n23m} = \int_0^b \lambda^e\left(\frac{y}{b}\right)\left(w^e_{,x}(a,y) - w^e_{,x2}\left(1-\frac{y}{b}\right) - w^e_{,x3}\left(\frac{y}{b}\right)\right)dy$$

$$\phi^e_{n34m} = \int_0^a \lambda^e\left(\frac{x}{a}\right)\left(w^e_{,y}(x,b) - w^e_{,y4}\left(1-\frac{x}{a}\right) - w^e_{,y3}\left(\frac{x}{a}\right)\right)dx$$

$$\phi^e_{n14m} = \int_0^b \lambda^e\left(\frac{y}{b}\right)\left(w^e_{,x}(0,y) - w^e_{,x1}\left(1-\frac{y}{b}\right) - w^e_{,x4}\left(\frac{y}{b}\right)\right)dy. \quad (46)$$

Substituting for $w^e_{,n}$ from eqn (32) into eqns (43) and (46) and performing the integrations gives

$$\boldsymbol{\phi}^e_n = \mathbf{W}^e_i \boldsymbol{\phi}^e_i + \mathbf{W}^e_j \boldsymbol{\phi}^e_j + \mathbf{W}^e_o, \tag{47}$$

where

$$\boldsymbol{\phi}^e_n = \{\phi^e_{n121}\ \phi^e_{n231}\ \phi^e_{n341}\ \phi^e_{n141} \cdots \cdots \phi^e_{n12M^*}\ \phi^e_{n23M^*}\ \phi^e_{n34M^*}\ \phi^e_{n14M^*}\} \tag{48}$$

and is made common to adjacent elements. The first two number subscripts in eqn (48) refer to the side number and the third number subscript refers to the harmonic number. If $M^* > 2$, $\mathbf{W}^e_j$ contains the first $M^* - 2$ rows and columns of $\mathbf{K}^e_{jj}$ as a submatrix. This is a consequence of the weighting functions chosen in eqns (43) and (46) and the sign convention used in equation (21). The terms in $\mathbf{W}^e_i$, $\mathbf{W}^e_j$ and $\mathbf{W}^e_o$ have been evaluated explicitly [10].

As the variables $\boldsymbol{\phi}^e_j$ are local to element e, eqn (47) can be solved for $\boldsymbol{\phi}^e_j$ to give

$$\boldsymbol{\phi}^e_j = \mathbf{W}^{e-1}_j (\boldsymbol{\phi}^e_n - \mathbf{W}^e_i \boldsymbol{\phi}^e_i - \mathbf{W}^e_o). \tag{49}$$

Substituting for $\boldsymbol{\phi}^e_j$ from eqn (49) into eqn (40) and neglecting a further constant gives

$$\Pi_p = \sum_e \left(\tfrac{1}{2} \{\boldsymbol{\phi}^e_i\ \boldsymbol{\phi}^e_n\}^T \begin{bmatrix} \bar{\mathbf{K}}^e_{ii} & \bar{\mathbf{K}}^e_{ij} \\ \bar{\mathbf{K}}^{eT}_{ij} & \bar{\mathbf{K}}^e_{jj} \end{bmatrix} \begin{Bmatrix} \boldsymbol{\phi}^e_i \\ \boldsymbol{\phi}^e_n \end{Bmatrix} - \{\boldsymbol{\phi}^e_i\ \boldsymbol{\phi}^e_n\}^T \begin{Bmatrix} \bar{\mathbf{R}}^e_i \\ \bar{\mathbf{R}}^e_j \end{Bmatrix} \right) \tag{50}$$

or

$$\Pi_p = \sum_e (\tfrac{1}{2} \bar{\boldsymbol{\phi}}^{eT} \bar{\mathbf{K}}^e \bar{\boldsymbol{\phi}}^e - \bar{\boldsymbol{\phi}}^{eT} \bar{\mathbf{R}}^e), \tag{51}$$

where

$$\begin{aligned}
\bar{\mathbf{K}}^e_{ii} &= \mathbf{K}^e_{ii} + \mathbf{W}^{eT}_i (\bar{\mathbf{K}}^e_{jj} \mathbf{W}^e_i - (\mathbf{W}^{e-1}_j)^T \mathbf{K}^{eT}_{ij}) - \mathbf{K}^e_{ij} \mathbf{W}^{e-1}_j \mathbf{W}^e_i \\
\bar{\mathbf{K}}^e_{ij} &= \mathbf{K}^e_{ij} \mathbf{W}^{e-1}_j - \mathbf{W}^{eT}_i \bar{\mathbf{K}}^e_{jj} \\
\bar{\mathbf{K}}^e_{jj} &= (\mathbf{W}^{e-1}_j)^T \mathbf{K}^e_{jj} \mathbf{W}^{e-1}_j \\
\bar{\mathbf{R}}^e_i &= \mathbf{R}^e_i - \mathbf{W}^{eT}_i (\bar{\mathbf{K}}^e_{jj} \mathbf{W}^e_o + (\mathbf{W}^{e-1}_j)^T \mathbf{R}^e_j) + \mathbf{K}^e_{ij} (\mathbf{W}^{e-1}_j)^T \mathbf{W}^e_o \\
\bar{\mathbf{R}}^e_j &= \bar{\mathbf{K}}^e_{jj} \mathbf{W}^e_o + (\mathbf{W}^{e-1}_j)^T \mathbf{R}^e_j
\end{aligned} \tag{52}$$

and $\bar{\boldsymbol{\phi}}^e = \{\boldsymbol{\phi}^e_i\ \boldsymbol{\phi}^e_n\}$. The matrix $\bar{\mathbf{K}}^e$ is symmetrical.

Setting the first variation of Π_p with respect to $\bar{\boldsymbol{\phi}}^e$ to zero gives

$$\sum_e (\bar{\mathbf{K}}^e \bar{\boldsymbol{\phi}}^e - \bar{\mathbf{R}}^e) = \mathbf{0}. \tag{53}$$

Equation (53) represents the stiffness equations for the elements in the region. Assembly and solution of the element stiffness equations follows standard finite element procedures. Only slight modifications are required to account for the variable element degrees of freedom.

With the elimination of the moment variables, the final variables are displacement parameters only. The elements are non-conforming other than at corners. As the number of terms in $\boldsymbol{\phi}^e_n$ is increased, the discontinuities in normal rotations between elements tend to zero. Hence as M^* tends to infinity the elements become conforming with C_1 continuity of displacements throughout.

BEAM ELEMENT

A variable degree of freedom element suitable to be coupled to the plate element is derived as follows. On, say, the side $y = 0$, the vertical displacement of the beam is taken as being compatible with the plate displacement on that side. Hence the displacement is expressed as a cubic polynomial in terms of the four polynomial parameters on that side plus a sine series in terms of the series displacement parameters on that side. The rotation of the beam about its longitudinal axis is expressed as a function of the two corner normal rotations of the side and the weighted integrals of normal rotations of the side.

The stiffness matrix for the beam is calculated from the strain energy of the beam under the assumptions of beam bending theory and St Venant's torsion theory. The beam stiffness matrices are added to the plate stiffness matrices to give the complete stiffness matrix for the structure. The detailed derivation of the beam stiffness matrix is given in [10].

OTHER ELEMENTS

Higher order polynomial elements

It has been noted that the polynomial shape functions $\mathbf{N}^e_p(x,y)$ in eqn (12) satisfy the homogeneous form of the governing differential equation. This automatically holds since each term used in developing the shape functions, namely 1, x, y, x^2, xy, y^2, x^3, x^2y, xy^2, y^3, x^3y and xy^3 is a biharmonic polynomial. Using additional biharmonic polynomials, e.g. $x^4 - x^2y^2$ and $y^4 - x^2y^2$, the number of polynomial functions in the displacement approximation may be increased, with the total displacement still satisfying eqn (7). This requires additional nodes on element sides to preserve C_0 continuity.

By increasing the number of polynomial functions in steps of four, an equal order of approximation may be maintained on all sides of the element. Details of elements using sixteen and twenty polynomial functions are given in [10]. The higher order polynomial functions however lead to increasingly complicated algebraic expressions for stiffness matrix terms. Alternatively, further elements can be derived by using different order of approximations on each side of the

element. This approach could be used to develop efficient elements with large aspect ratios or special transition elements to couple the macro elements with conventional elements.

Element with linear normal rotations

A twelve degree of freedom element with cubic displacements and linear normal rotations on the boundary of the element can be obtained as a special case of the proposed macro element. This element is derived by excluding the series displacement terms (i.e. taking $M = 0$) and setting $\phi_n^e = \mathbf{0}$ at the element level. As M^* is increased, the normal rotation on each side approaches a linear distribution. As the corner rotations are common to adjacent elements, the element becomes conforming as M^* approaches infinity. Note that this only occurs because the weighted integrals of normal rotations were defined according to eqn (43). If the definition of eqn (45) had been used, this derivation would not be possible.

The matrices for this element are obtained from eqn (50), giving the element equations

$$\bar{\mathbf{K}}_p^e \bar{\boldsymbol{\phi}}_p^e = \bar{\mathbf{R}}_p^e, \tag{54}$$

where $\bar{\mathbf{K}}_p^e$ and $\bar{\mathbf{R}}_p^e$ are the submatrices of $\bar{\mathbf{K}}_{ii}^e$ and $\bar{\mathbf{R}}_i^e$ in eqn (50) corresponding to the polynomial degrees of freedom $\bar{\boldsymbol{\phi}}_p^e$. This element can be viewed as a modified version of the ACM element with conforming displacements. The performance of this element is discussed below.

NUMERICAL RESULTS

A number of problems have been solved using the proposed elements to demonstrate the accuracy attainable. In all cases, Poisson's ratio was taken as 0.3 and, where applicable, the particular solution was taken as a Levy series solution truncated at 50 terms. In the following, the proposed macro element is designated MACPL and the modified ACM element is designated MACM. The boundary conditions are indicated by the symbols S (simple support, i.e. $w = M_n = 0$), C (clamped support, i.e. $w = w_{,n} = 0$) and F (free edge, i.e. $M_n = V_n = 0$). The first symbol description refers to the side $y = 0$, with the others following in a clockwise direction around the plate. For the single span plate example, the axes are taken as shown in Fig. 2.

Performance of MACPL element

A simply supported plate of dimensions $l \times d$ subjected to a uniform load was analysed using the proposed macro element. A quarter of the plate was analysed using a uniform mesh of N MACPL elements per side. It should be noted however that the obvious discretisation using the proposed macro element is to analyse the complete plate as a single element, which leads to the exact solution, namely $w = w_0$. In Table 1, the central deflection is compared with the exact value and in Table 2, the central moment is compared with the exact value for varying values of M and M^* and $N = 1$.

Table 1. Ratio of approximate to exact central displacement of SSSS plate under uniform load—MACPL element ($l/d = 1$, $N = 1$)

	M				
M^*	1	2	3	4	5
1	1.014	0.998	0.999	0.999	0.999
2	0.998	0.999	0.999	1.000	1.000
3	0.999	1.000	1.000	1.000	1.000
4	0.999	1.000	1.000	1.000	1.000
5	0.999	1.000	1.000	1.000	1.000

Table 2. Ratio of approximate to exact central moment of SSSS plate under uniform load—MACPL element ($l/d = 1$, $N = 1$)

	M				
M^*	1	2	3	4	5
1	1.063	0.950	0.976	0.976	0.976
2	0.950	1.006	1.068	1.016	1.016
3	0.976	1.019	0.998	0.995	0.998
4	0.976	1.016	0.995	1.004	1.005
5	0.997	1.016	0.998	1.005	1.000

It is clear that generally convergence to the exact solution only occurs as both M and M^* tend to infinity. Although the final variables are displacement parameters, convergence is not monotonic due to the mixed nature of the element approximations. Increasing M for a given M^* is generally a poor strategy. Although the order of the approximation of the boundary displacements increases, the discontinuity in the boundary normal boundary rotations is not reduced. Hence, errors are still present in the solution. To limit the total degrees of freedom required in practice, it appears from Tables 1 and 2 that the best convergence is achieved using $M = M^*$. Using this combination, convergence is rapid for both displacements and moments.

As noted above, the assumed element displacement function satisfies the governing differential equation. Convergence could be expected to be more rapid in element interiors than on element boundaries based on St Venant's principle. This is verified in Table 3, where the displacement and moment at the centre of the macro element modelling the quarter plate are shown for varying values of $M = M^*$. Both the displacement and moment rapidly approach the exact

Table 3. Ratios of approximate to exact quarter point displacement and moment of SSSS plate under uniform load—MACPL element ($l/d = 1$, $N = 1$)

$M = M^*$	Displacement	Moment
1	1.003	1.003
2	1.001	1.002
3	1.000	1.000
4	1.000	1.000
5	1.000	1.000

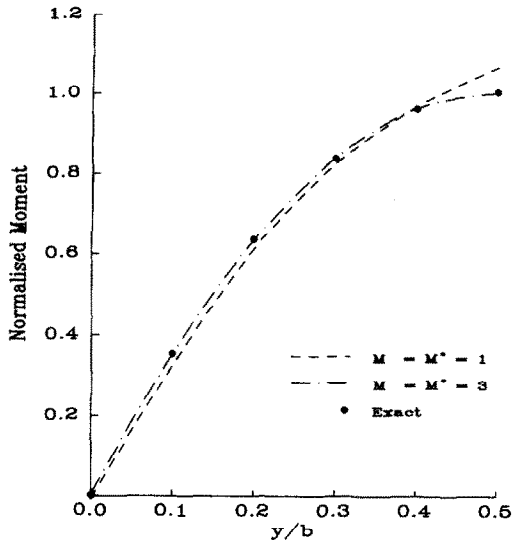

Fig. 4. Moment M_x at midspan of SSSS plate under uniform load—MACPL element ($l/d = 1$, $N = 1$).

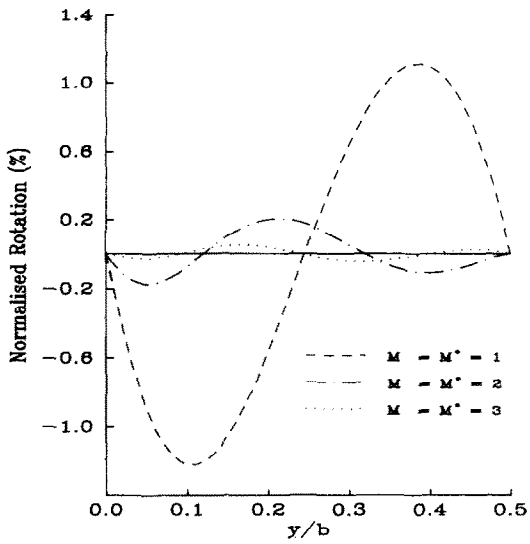

Fig. 6. Rotation $w_{,x}$ at midspan of SSSS plate under uniform load—MACPL element ($l/d = 1$, $N = 1$).

solution, with almost negligible errors for $M = M^* = 1$.

The moment M_x at midspan is shown in Fig. 4. Convergence is rapid with negligible errors when $M = M^* = 3$. The effective shear force at $x = 0$ is also accurately determined, as shown in Fig. 5.

The rotation $w_{,x}$ and the effective shear force at midspan are theoretically zero. The rotation can be exactly set to zero at the corners of the element corresponding to the points $(l/2, 0)$ and $(l/2, d/2)$. In addition, as M^* is increased, additional weighted integrals of $w_{,x}$ are set to zero. As M^* increases, the amplitude of $w_{,x}$ decreases and the curve oscillates with increased frequency about zero as shown in Fig. 6. The curve has been normalised by dividing by the exact value of $w_{,x}$ at the point $(0, d/2)$.

The condition of zero effective shear force at midspan is a natural boundary condition. Hence, the effective shear force is not set to zero at midspan, and tends to zero only in the limit as the number of series terms is increased. As M and M^* increase, the amplitude of the effective shear force decreases and the curve oscillates with increased frequency about zero, as shown in Fig. 7. The curve has been normalised by dividing by the exact value of the effective shear force at the point $(0, d/2)$.

The influence of the element aspect ratio, l/d, on the accuracy of the element is shown in Table 4. It can be seen from the table that the accuracy of the element does not deteriorate significantly as the aspect ratio is increased, although more series terms are required.

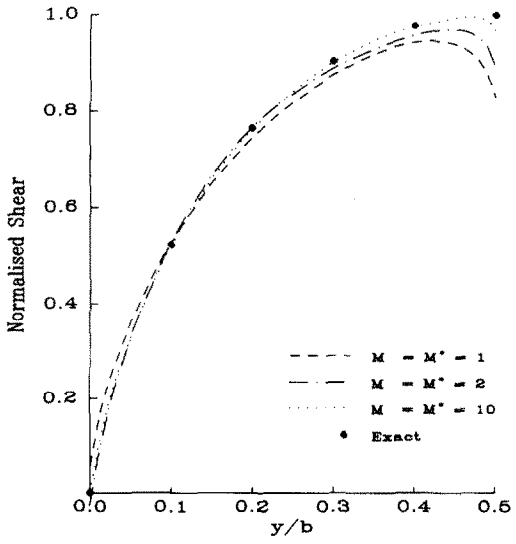

Fig. 5. Effective shear V_x at $x = 0$ of SSSS plate under uniform load—MACPL element ($l/d = 1$, $N = 1$).

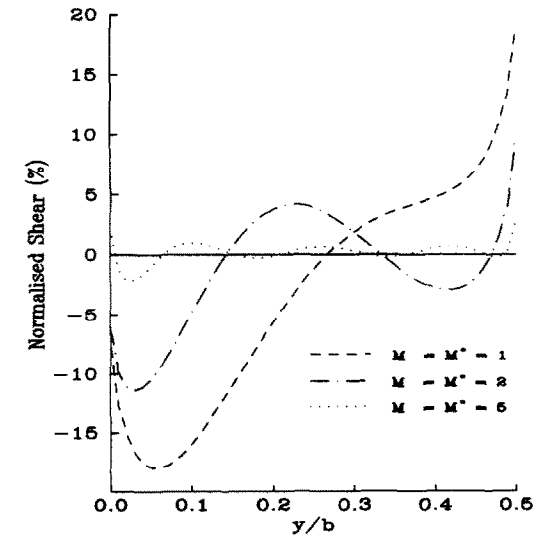

Fig. 7. Effective shear V_x at midspan of SSSS plate under uniform load—MACPL element ($l/d = 1$, $N = 1$).

Table 4. Ratio of approximate to exact central displacement of SSSS plate under uniform load—MACPL element ($N = 1$)

	l/d			
$M = M^*$	1	2	5	10
1	1.014	1.017	1.083	1.356
2	0.999	0.999	0.985	0.963
3	1.000	1.000	1.002	1.018
4	1.000	1.000	1.000	0.994
5	1.000	1.000	1.000	1.001

The effect of mesh refinement on the results is shown in Table 5. It can be seen that mesh refinement does not improve the performance. This is probably due to errors at element interfaces being introduced with mesh refinement. With single elements, internal errors do not occur as the governing differential equation is satisfied. Hence, using the minimum number of macro elements possible is a simple and effective strategy to adopt. The table also shows that the results for $M = M^* = 1$ are greatly inferior to the results for M and $M^* > 1$. Hence, it is recommended that a minimum of two series terms be used in all cases.

Table 5. Ratio of approximate to exact central displacement and moment of SSSS plate under uniform load—MACPL element ($l/d = 1$)

N	$M = M^*$	DOF†	Disp.	M_x
1	1	20	1.014	1.063
	2	28	0.999	1.006
	3	36	1.000	0.998
	4	44	1.000	1.004
	5	52	1.000	1.000
2	1	51	1.003	1.081
	2	75	1.000	0.999
	3	99	1.000	1.000
	4	123	1.000	1.001
	5	147	1.000	1.000
3	1	96	1.001	1.088
	2	144	1.000	0.999
	3	192	1.000	1.000
	4	240	1.000	1.000
	5	288	1.000	1.000

† Total degrees of freedom.

Table 6. Ratio of approximate to exact central displacement and moment of plate under uniform load—MACPL element ($l/d = 1$, $N = 1$)

	CCCC		FSFS	
$M = M^*$	Disp.	M_x	Disp.	M_x
1	1.102	1.038	1.002	1.048
2	0.998	1.028	1.000	1.012
3	0.999	0.985	1.000	1.004
4	1.000	1.014	1.000	1.004
5	1.000	0.997	1.000	1.002
10	1.000	1.002	1.000	1.001

Table 8. Ratio of approximate to exact central displacement of SSSS plate under uniform load—MACM and ACM elements ($l/d = 1$)

		M^*				
N	ACM	1	2	3	4	5
1	1.246	0.900	0.893	0.897	0.898	0.899
2	1.065	0.976	0.974	0.975	0.976	0.976
4	1.016	0.994	0.994	0.994	0.994	0.994
8	1.004	0.999	0.998	0.999	0.999	0.999
16	1.001	1.000	1.000	1.000	1.000	1.000

Results for uniformly loaded plates with other boundary conditions, and for plates subjected to point loads, are given in Tables 6 and 7. These results show a similar trend to the simply supported plate results. Convergence for point loading conditions is somewhat slower than for uniform loading. This is probably due to the singularity caused by the point load. In practice, the singularity would not occur as the load would be distributed over a small area.

Performance of MACM element

A simply supported square plate subjected to a uniform load was analysed using MACM and ACM elements. A quarter of the plate was discretised using a uniform mesh with N elements per side. The central deflection and central moment are shown in Tables 8 and 9 for varying values of N and M^*. The MACM element shows improved displacement convergence

Table 9. Ratio of approximate to exact central moment of SSSS plate under uniform load MACM and ACM elements ($l/d = 1$)

		M^*				
N	ACM	1	2	3	4	5
1	1.379	0.847	0.850	0.850	0.850	0.850
2	1.089	0.913	0.914	0.915	0.916	0.916
4	1.022	0.976	0.976	0.976	0.976	0.976
8	1.005	0.994	0.994	0.994	0.994	0.994
16	1.001	0.998	0.998	0.998	0.998	0.998

Table 7. Ratio of approximate to exact displacement and moments of plate under point load—MACPL element ($l/d = 1$, $N = 1$)

	SSSS		CCCC			FSFS	
$M = M^*$	w_1†	M_{x2}	w_1	M_{x2}	M_{x3}	w_1	M_{x2}
1	1.031	1.009	1.103	1.283	0.798	1.013	0.995
2	1.000	0.995	0.999	1.087	1.066	1.000	0.998
3	0.999	0.999	0.998	1.012	0.898	1.000	1.000
4	0.999	1.000	0.999	1.011	1.046	1.000	1.000
5	0.999	1.000	0.998	1.000	0.941	1.000	1.000
10	1.000	1.000	1.000	1.000	1.022	1.000	1.000

† Point 1 = $(l/2, d/2)$, 2 = $(l/4, d/4)$, 3 = $(0, d/2)$.

Table 10. Ratio of approximate to exact central displacement of plate under distributed load—MACM and ACM elements ($l/d = 1$)

	CCCC		FSFS	
N	Disp.	M_x	Disp.	M_x
(*a*) MACM *element* ($M^* = 2$)				
1	1.047	1.805	1.005	1.236
2	0.950	0.915	1.000	1.057
4	0.985	0.969	1.000	1.014
8	0.997	0.992	1.000	1.004
16	0.999	0.998	1.000	1.001
(*b*) ACM *element*				
1	1.169	2.015	0.985	1.172
2	1.109	1.213	0.992	1.042
4	1.030	1.050	0.998	1.010
8	1.008	1.012	0.999	1.003
16	1.002	1.003	1.000	1.001

Table 11. Ratio of approximate to exact displacement and moments of plate under point load—MACM and ACM elements ($l/d = 1$)

	SSSS		CCCC			FSFS	
N	w_1†	M_{x2}	w_1	M_{x2}	M_{x3}	w_1	M_{x2}
(*a*) MACM *element* ($M^* = 2$)							
1	0.852	0.791	0.945	0.000	1.012	0.979	0.990
2	0.959	0.878	0.926	2.140	0.839	0.990	1.040
4	0.989	0.897	0.977	2.153	0.928	0.997	0.985
8	0.997	0.974	0.994	1.293	0.977	0.999	0.996
16	0.999	0.993	0.998	1.077	0.994	1.000	0.999
(*b*) ACM *element*							
1	1.188	1.107	1.055	0.000	1.130	1.015	0.990
2	1.063	1.144	1.093	1.753	0.937	1.007	1.060
4	1.020	1.016	1.034	0.782	0.981	1.004	1.008
8	1.006	1.003	1.011	0.977	0.995	1.002	1.002
16	1.002	1.001	1.003	0.995	0.999	1.001	1.000

† Point 1 = ($l/2$, $d/2$), 2 = ($l/4$, $d/4$), 3 = (0, $d/2$).

over the ACM element by a factor of between two and three. The moment is more accurate for the MACM element for coarse meshes, while the ACM element performs better for finer meshes. For a given mesh (N = constant), displacements and moments converge rapidly to limiting values as M^* is increased. It is noted that the terms of the stiffness matrix for the MACM elements, which depend on M^*, converge rapidly to limiting values as M^* is increased, indicating that with $M^* = 2$ or 3, the variation of normal rotations on each element side is approximately linear.

Results for uniformly loaded plates with other boundary conditions, and for plates subjected to point loads, are given in Tables 10 and 11. Overall the MACM element shows some improvement over the ACM element.

Two-span continuous plate

As a final example, the two-span plate shown in Fig. 8 was considered. The plate was stiffened by edge beams with the rigidities shown in the figure. One span was subjected to a uniformly distributed load, q. One half of the section of the plate was analysed using two MACPL elements to provide a variety of boundary conditions. However, using these elements, the whole section could have been discretised using two elements without computational penalty. The half section was also analysed using ACM and MACM elements with a uniform 24 × 6 mesh. Displacements and moments at various locations are given in Table 12. The results demonstrate the capacity of the MACPL element to model large domains, and the rapid convergence that is achieved.

CONCLUSIONS

The proposed macro element enables the accurate solution of laterally loaded plates. The formulation is in terms of displacement parameters only, which enables plate and beam elements to be easily coupled. Large elements may be used, requiring a minimum of data preparation. Convergence is readily assessed by

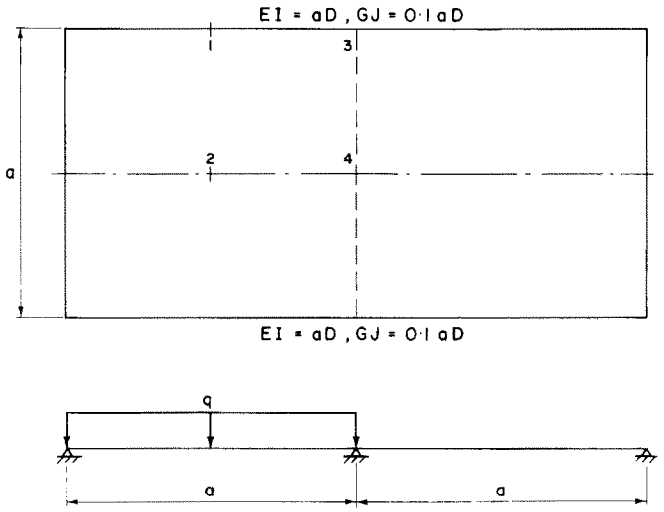

Fig. 8. Two-span continuous plate.

Table 12. Factors for two-span continuous plate

$M = M^*$	w_1	w_2	M_{x1}	M_{x2}	M_{x3}	M_{x4}
1	2.493	4.686	2.201	5.567	−1.440	−3.667
2	2.493	4.734	2.195	5.773	−1.349	−3.933
3	2.495	4.638	2.180	5.270	−1.345	−4.289
4	2.495	4.638	2.179	5.272	−1.324	−4.328
5	2.494	4.643	2.209	5.355	−1.316	−4.393
10	2.494	4.643	2.213	5.339	−1.293	−4.452
ACM	2.491	4.664	2.223	5.389	−1.297	−4.458
MACM ($M^* = 2$)	2.497	4.637	2.300	5.320	−1.301	−4.399
Multiplier	$10^{-3}qa^4/D$	$10^{-3}qa^4/D$	$10^{-2}qa^2$	$10^{-2}qa^2$	$10^{-2}qa^2$	$10^{-2}qa^2$

increasing the number of series terms, avoiding the necessity of defining a new mesh. Engineering accuracy for both displacements and stresses is generally obtained by using two or three series terms. In addition, a modified ACM element with linear normal rotations on the boundary has been shown to be a sub-element of the proposed macro element. This element shows some improvement in accuracy over the ACM element.

REFERENCES

1. M. M. Hrabok and T. M. Hrudley, A review and catalogue of plate bending finite elements. *Comput. Struct.* **19,** 479–495 (1984).
2. M. M. Hrabok and T. M. Hrudley, Finite element analysis in design of floor systems. *J. Struct. Engng, ASCE* **109,** 909–925 (1983).
3. O. C. Zienkiewicz, *The Finite Element Method,* 3rd Edn. McGraw-Hill, New York (1977).
4. F. K. Bogner, R. L. Fox and L. A. Schmit, The generation of interelement compatible stiffness and mass matrices by the use of interpolation formulae. *Proc. 1st. Conf. on Matrix Methods in Structural Analysis,* Wright Patterson Air Force Base, Ohio (Edited by S. S. Przemienicki *et al.*), pp. 397–443 (1965).
5. R. M. Gutkowski and C. K. Wang, Continuous plate analysis by finite panel method. *J. Struct. Engng, ASCE* **102,** 629–643 (1976).
6. B. W. Golley, A rectangular variable degree of freedom plate bending panel element. *Proc. 3rd. Int. Conf. In Australia on Finite Element Methods, Sydney* (Edited by A. P. Kaberle and V. A. Palmero), pp. 37–47. Unipart, Sydney (1979).
7. Z. Yan, Solution of plate structures by finite panel method. Nat. Conf. on Finite Element Methods, Nanning, China (1979).
8. Z. Yan, A mixed method of finite panel and its application. *Proc. Int. Conf. on Finite Element Methods, Shanghai, China* (Edited by H. Guangquiem and Y. K. Cheung), pp. 821–823. Gordon & Breach, New York (1982).
9. T. J. Parsons, H. V. S. GangaRao and W. C. Peterson, Macro-element analysis. *Comput. Struct.* **20,** 877–883 (1985).
10. J. Petrolito, Macro elements in stress analysis. Ph.D. Thesis, Dept. of Civil Engng, University College, University of New South Wales (1986).
11. S. Timoshenko and S. Woinowsky-Krieger, *Theory of Plates and Shells.* McGraw-Hill, New York (1959).
12. R. E. Jones, A generalisation of the direct stiffness method of structural analysis. *AIAA Jnl* **2,** 821–826 (1964).
13. T. H. H. Pian and P. Tong, Basis of finite elements for solid continua. *Int. J. Numer. Meth. Engng* **1,** 3–28 (1969).
14. J. W. Harvey and S. Kelsey, Triangular plate bending elements with enforced compatibility. *AIAA Jnl* **9,** 1023–1026 (1971).
15. P. Tong, New displacement hybrid finite element models for solid continua. *Int. J. Numer. Meth. Engng* **2,** 73–83 (1970).

APPENDIX

Series shape functions

$$\mathbf{N}_{tm} = \lfloor -(-1)^m f_1(a-x, b-y, a, b, m), \\ -(-1)^m f_1(b-y, x, b, a, m), \\ f_1(x, y, a, b, m), (-1)^m f_1(y, a-x, b, a, m) \rfloor$$

$$\mathbf{N}_{nm} = \lfloor (-1)^m f_2(a-x, b-y, a, b, m), \\ -(-1)^m f_2(b-y, x, b, a, m), \\ f_2(x, y, a, b, m), -f_2(y, a-x, b, a, m) \rfloor,$$

where

$$f_1(x, y, a, b, m) = \frac{\sin(\alpha_m x)}{2\alpha_m s^2 D}(y\cosh(\alpha_m y)s - b\sinh(\alpha_m y)c)$$

and

$$f_2(x, y, a, b, m) \\ = \frac{\sin(\alpha_m x)}{2s^2}(\alpha_m b \sinh(\alpha_m y)(1-\nu)c \\ + \alpha_m y \cosh(\alpha_m y)s(\nu - 1) + 2\sinh(\alpha_m y)s).$$

Transformation matrix

$$\mathbf{A}_m = \begin{bmatrix} \alpha_m & 0 & 0 & 0 \\ 0 & 0 & 0 & \beta_m \\ (-1)^m\alpha_m & 0 & 0 & 0 \\ 0 & \beta_m & 0 & 0 \\ 0 & 0 & (-1)^m\alpha_m & 0 \\ 0 & (-1)^m\beta_m & 0 & 0 \\ 0 & 0 & \alpha_m & 0 \\ 0 & 0 & 0 & (-1)^m\beta_m \end{bmatrix}.$$

In the above formulas, $s = s(a, b, m) = \sinh(\alpha_m b)$, $c = c(a, b, m) = \cosh(\alpha_m b)$, $\alpha_m = \alpha_m(a, m) = m\pi/a$ and $\beta_m = \beta_m(m, b) = m\pi/b$.